Pertanika J. Trop. Agric. Sci. 49 (5): 2217 - 2236 (2026)

PERTANIKA JOURNALS

TROPICAL AGRICULTURAL SCIENCE

Journal homepage: http://www.pertanika.upm.edu.my/

Gallic Acid-Loaded Graphene Oxide (GAGO) Nanocomposite Attenuates Inflammatory Response in LPS-Stimulated RAW 264.7 Macrophages

Nur Hazwani Norjoshukrudin[1], Ida May Jen Ng[1], Seri Narti Edayu Sarchio[2], Masriana Hassan[3], Shafinaz Abd Gani[1], and Suhaili Shamsi[1,4]*

[1]Animal Biochemistry and Biotechnology Laboratory, Department of Biochemistry, Faculty of Biotechnology and Biomolecular Sciences, Universiti Putra Malaysia, 43400 Serdang, Selangor, Malaysia
[2]Department of Biomedical Science, Faculty of Medicine and Health Sciences, Universiti Putra Malaysia, 43400 Serdang, Selangor, Malaysia
[3]Department of Pathology, Faculty of Medicine and Health Sciences, Universiti Putra Malaysia, 43400 Serdang, Selangor, Malaysia
[4]Natural Medicine and Product Research Laboratory, Institute of Bioscience, Universiti Putra Malaysia, 43400 Serdang, Malaysia

ABSTRACT

Reckless use of non-steroidal anti-inflammatory drugs (NSAIDs) has contributed to adverse health effects. In the present study, a gallic acid-loaded graphene oxide (GAGO) nanocomposite was synthesised, and its cytotoxicity and anti-inflammatory properties were evaluated in vitro. GAGO was first synthesised and characterised using FTIR, FESEM, and zeta potential analyses. The gallic acid (GA) loading efficiency of GAGO was quantified, while stability was monitored following 90 days of storage at room temperature. NIH-3T3 fibroblast and RAW 264.7 macrophage cells were employed to evaluate the cytotoxicity of GAGO in vitro. Finally, the anti-inflammatory properties were assessed by measuring nitric oxide (NO) and pro-inflammatory cytokine levels, namely IL-6, TNF-α, and MCP-1, in LPS-induced RAW264.7 macrophages. GA was successfully loaded into GAGO at a loading efficiency of 51.07% ± 7.27% and remained stable upon storage for 90 days. GAGO exhibited a significantly improved in vitro cytotoxicity compared to GA, with LC50 values of 28.95 ± 6.674 µg/mL in NIH-3T3 cells, and 60.23 ± 0.168 µg/mL in RAW 264.7 cells at 72 h. GA significantly increased NO production at higher concentrations (≥30 µg/mL), indicating

ARTICLE INFO

Article history:
Received: 21 October 2025
Accepted: 25 September 2026
Published: 30 October 2026

DOI: https://doi.org/10.47836/pjtas.49.5.06

E-mail addresses:
nurhazwaninorjo@gmail.com (Nur Hazwani Norjoshukrudin)
idangmj@gmail.com (Ida May Jen Ng)
serinarti@upm.edu.my (Seri Narti Edayu Sarchio)
masriana@upm.edu.my (Masriana Hassan)
shafinaz_abgani@upm.edu.my (Shafinaz Abd Gani)
sh_suhaili@upm.edu.my (Suhaili Shamsi)
* Corresponding author

© Universiti Putra Malaysia Press

a potential pro-oxidant effect. In contrast, GAGO significantly suppressed the NO level at a low concentration (5 μg/mL), while no significant increase was observed at higher concentrations compared to the LPS-induced control. Furthermore, GAGO reduced IL-6 (45-60 μg/mL), TNF-α (≥15 μg/mL) and MCP-1 (≥10 μg/mL) levels, comparable to GA. The present study highlights the potential of GAGO nanocomposite to attenuate inflammation, but further mechanistic and in vivo investigations are warranted.

Keywords: GAGO, Gallic acid, graphene oxide, inflammation, nanoformulation

INTRODUCTION

Inflammation, the body's first initial response to injury or infection, is often mitigated by the administration of non-steroidal anti-inflammatory drugs (NSAIDs) (Gunaydin & Bilge, 2018). However, excessive and prolonged use of NSAIDs has contributed to serious adverse effects, which include gastrointestinal disorders like peptic ulcers (Tai & McAlindon, 2021), chronic kidney disease (CKD) (Drożdżal et al., 2021), and hepatotoxicity (Sriuttha et al., 2018). NSAIDs could also compromise the immune system, making it more susceptible to infection, which accelerates the emergence of antibiotic-resistant organisms (Chen et al., 2021; Li et al., 2023b).

In recent years, various studies have focused on identifying alternative treatments for inflammation, which is typically treated with NSAIDs. Phenolic compounds have garnered interest as potential alternatives to conventional NSAIDs due to their non-toxic nature and therapeutic potential in modulating various signalling pathways and stimulating various mechanisms of action (Arip et al., 2022; Sohrabi et al., 2021; Srivastava et al., 2014; Wang et al., 2020). A naturally derived phenolic compound, namely gallic acid (GA), has attracted the attention of many researchers for its ability to exhibit myriad pharmacological activities. This simple phenolic compound has demonstrated antioxidant (Jiang et al., 2024), anti-cancer (Ashrafizadeh et al., 2021), anti-microbial (Shamsi et al., 2018; Shamsi et al., 2022), and anti-inflammatory (Li et al., 2023a) activities in various in vitro and in vivo models (Reckziegel et al., 2016). Nevertheless, like many other naturally derived phenolic compounds, GA undergoes rapid degradation (Chikere et al., 2020) and is deemed unstable at pH above 7 and at high temperatures (Pasquet et al., 2024). GA is rapidly metabolised (Zhang et al., 2020), and, when combined with poor absorption, this results in low bioavailability and immediate clearance of GA following in vivo administration (Bai et al., 2021; Mao et al., 2016).

Numerous studies have then shifted their focus to improving the physicochemical properties of GA, including the use of nanoparticles as a delivery platform for GA. Nanoparticles have been shown to enhance bioavailability, improve stability, and enable targeted, controlled-release delivery (Díez-Pascual, 2021; Petrovic et al., 2024).

Nanoparticles have also been shown to possess prominent anti-inflammatory properties, through modulation of inflammatory mediators involved in inflammation, including nitric oxide (NO) and key pro-inflammatory cytokines, such as interleukin-6 (IL-6), tumour necrosis factor-α (TNF-α), and monocyte chemoattractant protein-1 (MCP-1) (Mi et al., 2022). One prominent example is curcumin-loaded nanoparticle systems that have been reported to suppress NO production and reduce the secretion of pro-inflammatory cytokines, including IL-6 and TNF-α, in activated macrophages through inhibition of nuclear factor-κB (NF-κB) signalling pathways (Chopra et al., 2021; Laurindo et al., 2023). Similarly, resveratrol-loaded nanocarriers have demonstrated significant inhibition of inflammatory mediators, including TNF-α and NO, by modulating inflammatory transcription factors (Grabarczyk et al., 2024; Siu et al., 2018). In addition, quercetin-encapsulated nanoparticles have been shown to attenuate inflammatory responses via sustained inhibition of the PI3K/Akt pathway (Lou et al., 2016). Collectively, these findings highlight the potential of nanoparticle-based delivery systems to enhance the therapeutic potential of bioactive compounds, including GA, for the management of inflammatory conditions, although their safety and efficacy require further investigation.

A nanocomposite formulation developed in our laboratory, GA-loaded graphene oxide (GAGO) nanocomposite, has previously demonstrated a significant anti-bacterial effect, as well as wound healing properties with an improved toxicity profile, making it a potential candidate for therapeutic applications (Azhari, 2023; Shamsi et al., 2018; 2020). GAGO exhibited improved toxicity profile compared to native GA and graphene oxide (GO) (Ghafor et al., 2020). Further research by Shamsi et al. (2022) investigated the antibacterial properties of GAGO against community and hospital-acquired methicillin-resistant Staphylococcus aureus (MRSA). They found that during the first two hours of bacterial exposure, the effectiveness of GAGO was comparable to that of GA and GO alone. At concentrations of ≥150 μg/mL, GAGO demonstrated antibacterial activity comparable to the conventional antibiotic, cefoxitin.

Bacterial infections and chronic wounds can lead to elevated inflammation; the next logical step in developing GAGO for clinical settings is to explore its anti-inflammatory potential. The present study endeavours to explore GAGO's potential to exert anti-inflammatory effects in an in vitro cell model using the established RAW 264.7 macrophage cell line induced with bacterial lipopolysaccharide (LPS). This study hopes to provide a potential alternative to NSAIDs with a view to developing GAGO nanocomposite as a multifunctional therapeutic with anti-inflammatory properties.

MATERIALS AND METHODS

Materials

All experiments performed in the present study utilised analytical grade chemicals and reagents. Graphite (Gr) powder procured from Fluka Chemical (Buchs, Switzerland)

was used as the starting material for GO synthesis. GA, sodium hydroxide (NaOH), hydrochloric acid (HCl), potassium permanganate ($KMnO_4$), phosphoric acid (H_3PO_4), sulphuric acid (H_2SO_4), diethyl ether, sodium dodecyl sulphate (SDS), sulphanilamide, N-1-naphthyl-ethylenediamine hydrochloride (NED), 3-[4,5-dimethylthiazol-2-yl]-2,5 diphenyl tetrazolium bromide (MTT) reagent, and phosphate buffered saline (PBS) were purchased from Sigma-Aldrich (Missouri, USA). Dulbecco's Modified Eagle's medium (DMEM) purchased from Nacalai Tesque (Kyoto, Japan) was supplemented with fetal bovine serum (FBS) from Tico Europe (South Holland, Netherlands) for cell culture maintenance. Penicillin, streptomycin, and trypsin-EDTA were obtained from Nacalai Tesque (Kyoto, Japan).

Synthesis and Characterisation of GAGO Nanocomposite

GO was accordingly synthesised using an Improved Hummer's method (Marcano, 2010). GAGO synthesis was conducted according to our previously developed method (Shamsi et al., 2018). GA and GO were mixed at a weight ratio of 5:1 in distilled water and stirred overnight. This was followed by centrifugation for 15 min at 4000 rpm. The mixture was washed three times successively with distilled water and subsequently dried at 40 °C (Memmert GmbH + Co.KG, Schwabach, Germany). For morphological observation of GO and GAGO, field-emission scanning electron microscopy (FESEM) equipped with energy-dispersive X-ray spectroscopy (EDX) for elemental analysis was employed. Presence of functional groups in GO and GAGO was monitored under Fourier-transform infrared spectroscopy (FTIR) (Shimadzu, Tokyo, Japan), alongside Gr and GA that served as controls. Dynamic light scattering (DLS) (Malvern Instruments, Worcestershire, United Kingdom) was utilised to measure the zeta potential of GO and GAGO nanocomposite. A previously developed method was used to quantify GA loading in the synthesised GAGO nanocomposite (Shamsi et al., 2022). Storage stability of the GAGO nanocomposite was monitored for 90 days at room temperature by evaluating the zeta potential and GA loading at specific time intervals (0, 7, 14, 21, 28, 60, and 90 days).

Cell Culture

NIH-3T3 fibroblast cells and RAW 264.7 macrophage cells obtained from the American Type Culture Collection (ATCC) were maintained in DMEM supplemented with 10% FBS and 1% penicillin-streptomycin. Cells were cultured at 37 °C in a humidified incubator (90% humidity) with a continuous supply of 5% CO2 (Nuaire, Minnesota, USA).

In Vitro Cytotoxicity Assay

A cytotoxicity study was conducted on both NIH-3T3 fibroblasts and RAW 264.7 macrophages using the MTT assay. Cells were seeded onto 96-well plates (NIH-3T3 cells

at 4×10^5 cells/mL and RAW 264.7 cells at 1.25×10^5 cells/mL) in 200 µL of supplemented DMEM. Upon confluency, cells were washed once with pre-warmed basal DMEM, followed by incubation with respective samples at concentrations of 0-1000 µg/mL (GO, GA and GAGO). Cells exposed to 0.1% w/v SDS served as the positive control, while cells exposed only to culture medium served as the negative control. Cells were treated with samples for 24 to 72 h, with fresh samples replenished at 24 h intervals. At the end of the incubation time, cells were then incubated with MTT reagent at 0.5 mg/mL for 4 h. The purple formazan crystal formed following incubation with MTT reagent was solubilised with DMSO (100 µL), and the absorbance values were recorded at 570 nm using a multiplate spectrophotometer (Multiskan FC, Thermo Fisher Scientific, Massachusetts, USA). The LC_{50} values for all samples were determined accordingly (Seisenbaeva et al., 2021).

LPS Stimulation in RAW 264.7 cells

Cells were seeded at a density of 1×10^5 cells/mL in phenol red-free DMEM containing only 2% FBS in a 24-well plate. Cells were induced with LPS from *Escherichia coli* 0111: B4 (ENZO Life Sciences, USA) at 1 µg/mL for 2 h (Zailan et al., 2020). The cells were then treated for 24 h with 0-60 µg/mL of the respective samples (GO, GA, or GAGO). Upon reaching 24 h of treatment, 500 µL of the cell supernatant was retrieved and stored in a -80 °C freezer until further use for Griess and cytometric beads array (CBA) assays.

Griess Assay

Cell supernatant (50 µL) was transferred into a 96-well plate, with the addition of 50 µL of Griess reagent containing 1% sulphanilamide and 0.1% N-1-naphthyl-ethylenediamine hydrochloride prepared with 2.5% of phosphoric acid. The absorbance value was recorded after 15 min incubation in the dark at 540 nm (Zailan et al., 2020). The level of NO in the cell supernatant was determined using a standard curve ($y = 0.0038x-0.0019$, $R^2 = 0.9986$) of sodium nitrate solution prepared at different concentrations (0-20 µM).

Determination of Cytokine Level using the Cytometric Beads Array (CBA) Assay

The levels of IL-6, TNF-α, and MCP-1 in LPS-induced RAW 264.7 cells were measured following treatment with GO, GA or GAGO (0-60 µg/mL) using the CBA assay. CBA assay was conducted according to the guidelines provided by the manufacturer (BD™ CBA Mouse Inflammation Kit from BD Biosciences, California, USA). Supernatant containing cells was added to 50 µL of mixed capture beads and phycoerythrin (PE) detection reagent and incubated in the dark for 2 h. Wash buffer was added, and the mixture was centrifuged for 5 min at 200 × g to obtain the pellet. Following this, cytokine levels were measured using

a flow cytometer (BD FACSCanto, BD Biosciences, USA). Results were generated and analysed using the FCAP Array™ Software (BD Biosciences, USA) (Zailan et al., 2020).

Statistical Analysis

All data ($n \geq 3$) are presented as mean ± standard deviation (SD). Data were statistically analysed by employing a One-Way or Two-Way Analysis of Variance (ANOVA) with Tukey's post hoc, unless otherwise stated (GraphPad Prism Version 9.0, GraphPad Software, California, USA). A p-value of ≤ 0.05 is considered statistically significant.

RESULTS

Synthesis and Characterisation of GAGO Nanocomposite

In Figure 1A, the black fine powder of GO was obtained, while the GAGO nanocomposite appears as a thin black film upon drying overnight at 40°C (Figure 1B). All samples were characterised by FTIR to determine the presence of functional groups (Figure 1C). Gr and GA analyses were also conducted as a control. According to Figure 1C, all black arrows represent new peaks that correspond to the characteristic peaks of GA, which are present in the GAGO nanocomposite. The first characteristic peak for GAGO was observed at 1375 cm^{-1}, which corresponds to the O-H plane bending functional group in GA. The second characteristic peak for GAGO occurs at 1444 cm^{-1}, which corresponds to the aromatic ring C=C stretching functional group in GA. The third characteristic peak for GAGO was at 3769 cm^{-1}, and this corresponds to the characteristic peak of the benzene ring O-H stretching of GA. Collectively, the FTIR spectrum of GAGO nanocomposite displays characteristic peaks of functional groups present in GO and GA, respectively, indicating successful loading of GA onto GO to form the GAGO nanocomposite. FESEM observations were conducted to assess differences in the morphology of GAGO compared with GO. Based on Figure 1D, it was revealed that GO appears as a wrinkled thin film, while GAGO appears thicker and denser, with an apparent crystalline structure, indicating the presence of GA (Figure 1E), which aligns with a previous study from our laboratory (Shamsi et al., 2022).

Figure 2A-2D presents the EDX spectra of all samples, including Gr and GA as controls, together with their corresponding FESEM micrographs. The EDX spectrum of Gr was dominated by carbon (C), with a minor oxygen (O) signal and low-intensity peaks corresponding to Fe, Mg, Si and Ca. These additional elemental signals may be attributed to trace mineral impurities associated with the Gr precursor. Previous studies have reported the presence of mineral inclusions containing Fe, Mg, Si and Ca in natural Gr, including silicate and carbonate minerals such as pyroxene, quartz, calcite and dolomite (Kumara et al., 2021). The low intensities of these signals suggest that these elements are minor constituents of the analysed Gr rather than its predominant components.

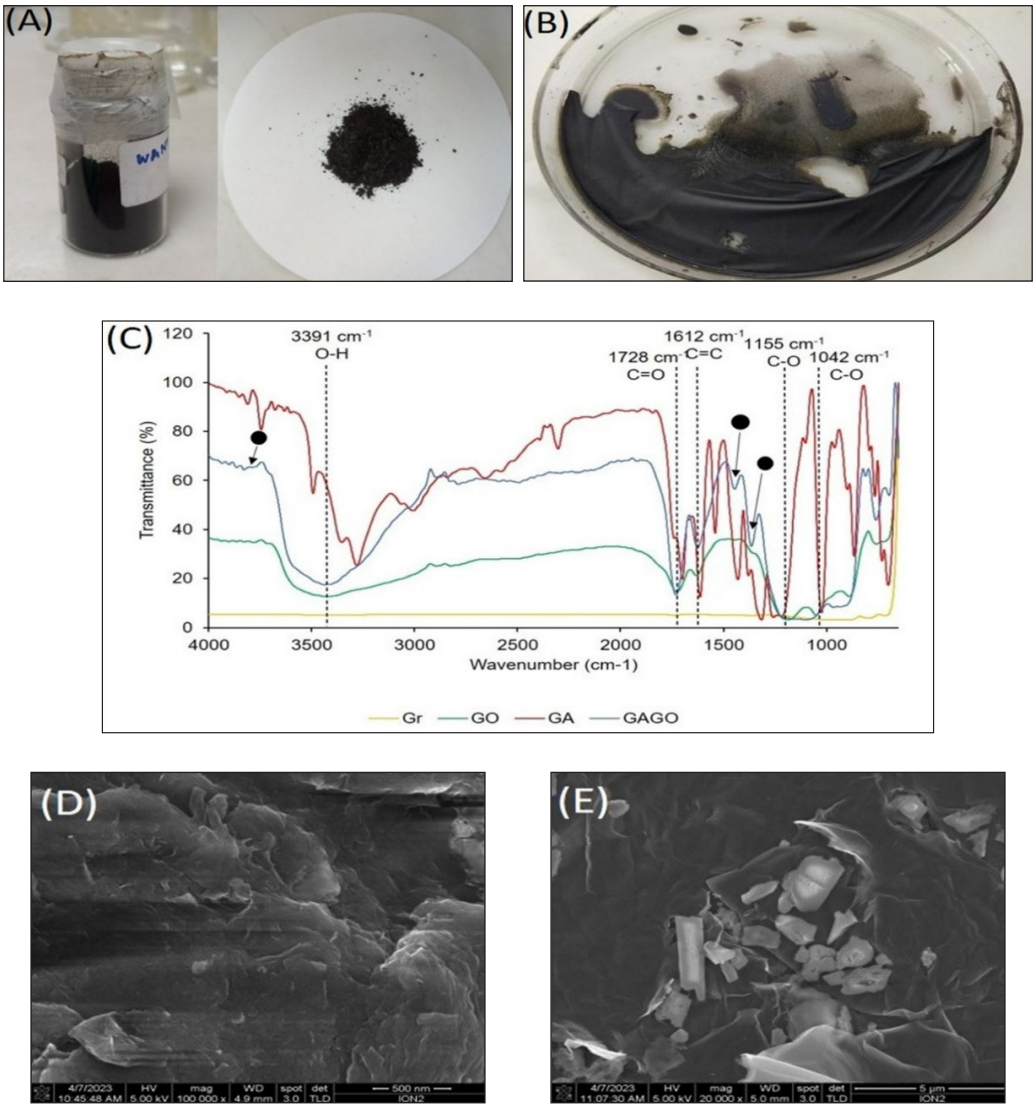

Figure 1. Characterisation of GO and GAGO nanocomposite. (A) GO powder obtained via a modified Hummer's method, (B) GAGO nanocomposite thin film prepared at a 1:5 w/w ratio of GA to GO, (C) FTIR spectra of GAGO, GO, GA, and Gr

Note. Black spots indicate characteristic peaks in the GAGO spectrum corresponding to GA. (D) FESEM micrograph of GO with a scale bar of 500 nm, and (E) FESEM micrograph of GAGO with a scale bar of 5 µm

As presented in Table 1, the C content of Gr was higher than that of GO (41.36%) and GAGO (49.90%), whereas the O content increased substantially from 6.51% in Gr to 47.09% in GO and 41.95% in GAGO. The reduction in the relative C content and the corresponding increase in O content following oxidation are consistent with the introduction of oxygen-containing functional groups during GO synthesis. These functional groups include hydroxyl, epoxy, carbonyl and carboxyl groups, which contribute to the oxygen-rich

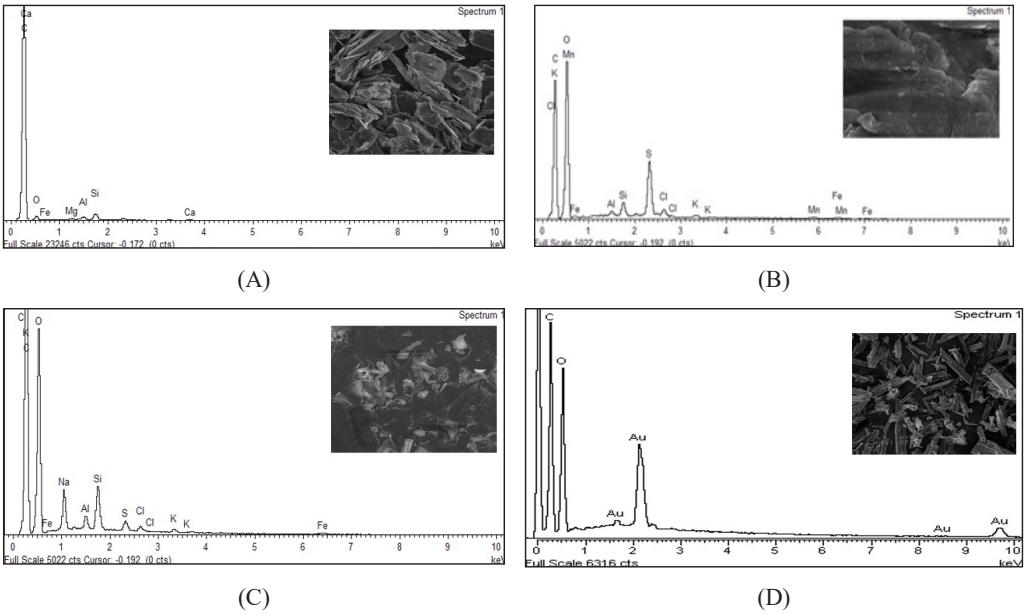

Figure 2. EDX spectra with corresponding FESEM micrographs (insets) of (A) Gr, (B) GO, (C) GAGO, and (D) GA. Prominent carbon (C) and oxygen (O) peaks are observed in GO and GAGO, confirming successful oxidation of Gr and the presence of oxygen-containing functional groups. GAGO exhibits higher C content than GO. Minor peaks corresponding to S, Cl, Mn, and other residual elements originate from the oxidation process during GO synthesis. The Au peaks observed in selected spectra are attributed to gold sputter coating during FESEM sample preparation

Table 1
Elemental analysis of Gr, GO, GAGO, and GA according to EDX

Element Weight (%)	Gr	GO	GAGO	GA
C	90.71	41.36	49.90	44.15
O	6.51	47.09	41.95	53.16
S	-	6.86	0.79	-
Cl	-	1.11	0.42	-
Al	0.50	0.36	0.71	-
Si	1.28	1.19	2.54	-
K	-	0.37	0.38	-
Mn	-	0.75	-	-
Fe	0.50	0.90	0.58	-
Ca	0.29	-	-	-
Mg	0.22	-	-	-
Na	-	-	2.73	-

Note. Trace elements detected in the samples, including S, Cl, Si, K, Mn, Fe, Ca, Mg, and Na, may have originated from the synthesis and sample preparation processes or from the reagents and materials used. These elements were not considered part of the intended elemental composition

composition of GO. Following GA loading, GAGO exhibited an increase in relative C content from 41.36% in GO to 49.90%, accompanied by a decrease in O content from 47.09% to 41.95%. These changes are consistent with the incorporation of GA, which contains both C and O, into the GO matrix. The higher relative C content of GAGO may be associated with the contribution of C from the loaded GA.

In addition to C and O, the EDX spectra of GO and GAGO revealed minor signals corresponding to Si, S, Cl and K. The presence of these elements may be associated with residual inorganic species originating from the Gr precursor, as well as the GO synthesis and purification processes. Specifically, S (6.86% in GO and 0.79% in GAGO) may be associated with residual sulphate-containing species from the use of H_2SO_4, while K may originate from $KMnO_4$, used as the oxidising agent during GO synthesis. Similarly, Cl (1.11% in GO and 0.42% in GAGO) may be associated with residual chloride-containing compounds when HCl was used during synthesis. The detection of Si may reflect mineral impurities inherited from the Gr precursor. The persistence of these elements in GAGO suggests that some of the minor elemental constituents detected in GO were retained following GA loading. In contrast, the EDX spectrum of GA exhibited only C and O signals, consistent with its expected elemental composition and supporting its high apparent elemental purity.

The additional Al and Au signals detected in the EDX spectra are attributed to the materials used during FESEM sample preparation. Specifically, the Al signal may originate from the aluminium stub used to mount the samples, particularly where the sample coating does not completely cover the underlying substrate. The Au signals observed in selected spectra are associated with the gold sputter coating applied to improve electrical conductivity and minimise charging during FESEM imaging. Therefore, these signals are considered preparation-related contributions rather than intrinsic elemental constituents of the analysed samples.

GA has been successfully loaded at 0.425 ± 0.06 g of GAGO, with a loading efficiency of 51.07% ± 7.27%. Additionally, the batch-to-batch consistency in terms of the yield and GA loading was confirmed in more than 3 batches ($n \geq 3$) of the synthesised GAGO nanocomposite. The stability of the GAGO nanocomposite during storage was monitored for GA loading and zeta potential under the following conditions: at room temperature in a sealed glass bottle, away from moisture and light. Figure 3A shows that no significant reduction in GA loading was observed until D90 ($p \leq 0.05$), despite a 68.50% ± 12.93% reduction. In addition to this, GAGO has also exhibited no significant reduction in the zeta potential after 90 days of storage ($p \leq 0.05$) (Figure 3B). Prolonged storage stability study, ideally up to 12 months, should be conducted to evaluate the suitable shelf life for the nanocomposite produced, prior to GAGO being introduced in the clinical settings.

Cytotoxicity of GA, GO, and GAGO in NIH-3T3 and RAW 264.7 cells

The LC_{50} values following treatment of NIH-3T3 and RAW 264.7 cells with samples of GO, GA, and GAGO were determined, as shown in Figure 4A and 4B, respectively. GA demonstrated lower LC_{50} values than GO and GAGO at all incubation times. GA displayed a higher toxicity in both cell lines, causing a 50% reduction in cell viability at 38.26 ± 8.549 µg/mL (Figure 4A) and 73.98 ± 0.146 µg/mL (Figure 4B) at 24 h. Based on Figure 4A, GAGO displayed higher LC_{50} values than GA at all incubation times, decreasing from 245.30 ± 9.867 µg/mL at 24 h, 78.91 ± 9.172 µg/mL at 48 h, and 28.95 ± 6.674 µg/mL at 72 h. Similarly, in RAW 264.7 macrophage cells (Figure 4B), GAGO demonstrated higher LC_{50} values compared to GA, reducing from 387.00 ± 0.189 µg/mL at 24 h, 71.75 ± 0.149 µg/mL at 48 h, and 60.23 ± 0.168 µg/mL at 72 h.

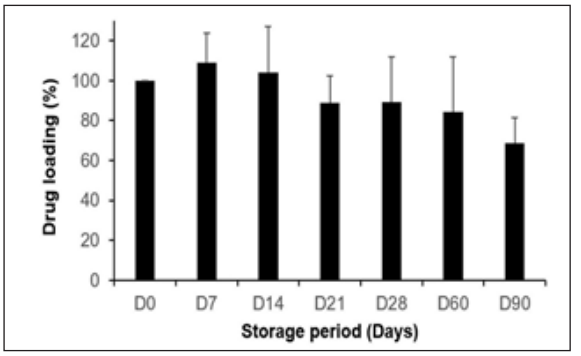

(A)

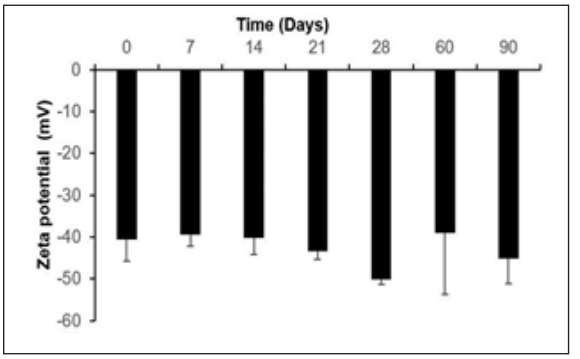

(B)

Figure 3. Storage stability of GAGO. (A) Drug loading (%) and (B) zeta potential values of GAGO after storage for 90 days ($n \geq 3$ different batches). No significant difference was observed in drug loading (GA) and zeta potential values at all storage periods compared to D0 ($p \leq 0.05$)

NO Level in LPS-induced RAW 264.7 Cells

Figure 5 illustrates the levels of NO produced in RAW 264.7 cells induced with 1 µg/mL of LPS, following treatment for 24 h with GA, GO, and GAGO samples at a concentration range of 0-60 µg/mL. The uninduced and untreated cells at 0 µg/mL served as controls. As shown in Figure 5, treatment with GA has increased the NO level in a concentration-independent manner, with a significant increase compared to control observed at higher concentrations (30, 45, and 60 µg/mL). In contrast, GO did not significantly increase the NO level. The NO levels remained relatively stable, indicating that GO did not promote inflammatory activation under these conditions. Conversely, in LPS-induced cells treated with GAGO, a significant reduction of NO level was observed at 5 µg/mL.

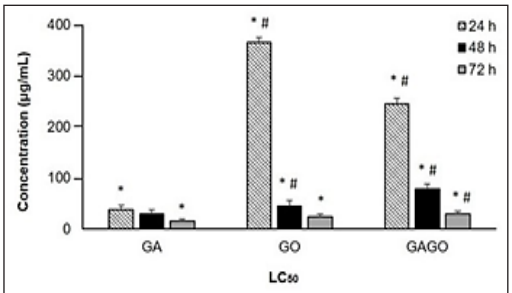

Exposure time (h)	LC50 (µg/mL)		
	GA	GO	GAGO
24	38.26 ± 8.549	364.10 ± 10.670	245.30 ± 9.867
48	29.62 ± 7.781	44.37 ± 11.190	78.91 ± 9.172
72	15.29 ± 4.424	24.52 ± 5.092	28.95 ± 6.674

(A)

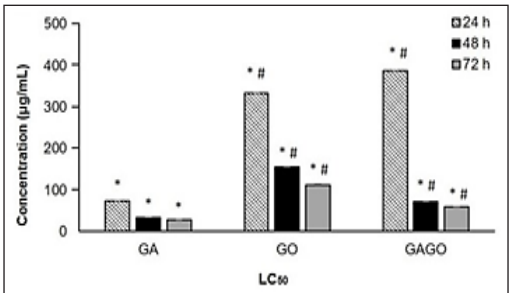

Exposure time (h)	LC50 (µg/mL)		
	GA	GO	GAGO
24	73.98 ± 0.146	334.10 ± 0.164	387.00 ± 0.189
48	33.89 ± 0.108	155.50 ± 0.168	71.75 ± 0.149
72	27.74 ± 0.094	112.90 ± 0.123	60.23 ± 0.168

(B)

Figure 4. LC_{50} values in (A) NIH-3T3 fibroblast cells and (B) RAW 264.7 macrophage cells following treatment with GA, GO and GAGO at 24, 48, and 72 hours

Note. The (*) symbol indicates a significant difference between 24 and 72 hours within the same sample, while the (#) symbol denotes a significant difference compared to GA at the same time point ($p \leq 0.05$). Data are presented as mean ± SD ($n \geq 3$)

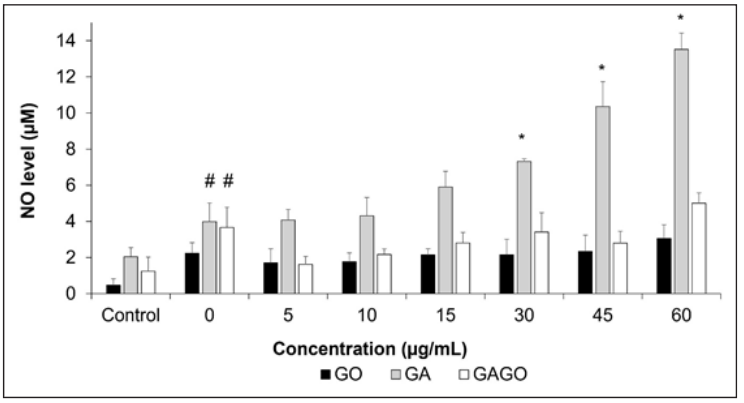

Figure 5. NO levels in LPS-induced RAW 264.7 macrophage cells following treatment with GO, GA and GAGO for 24 h. Cells were induced with 1 µg/mL of LPS for 2 h, followed by treatment of the cells with the respective samples at concentrations of 0-60 µg/mL for 24 h

Note. The (*) symbol denotes a significant difference compared to 0 µg/mL ($p \leq 0.05$), whereas the (#) symbol denotes a significant difference between control uninduced cells (Control) and 0 µg/mL ($p \leq 0.05$) ($n = 3$)

Inflammatory Cytokine Levels in RAW 264.7 Cells

Figure 6 shows the level of IL-6, TNF-α, and MCP-1 in LPS-induced RAW 264.7 macrophage cells after 24 h of treatment with GA, GO, and GAGO. IL-6, TNF-α, and

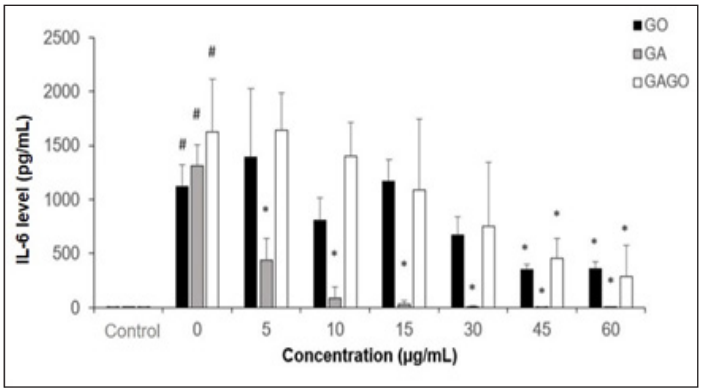

(A)

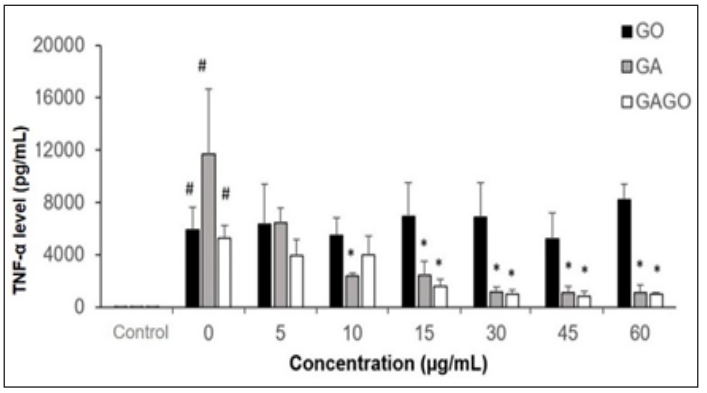

(B)

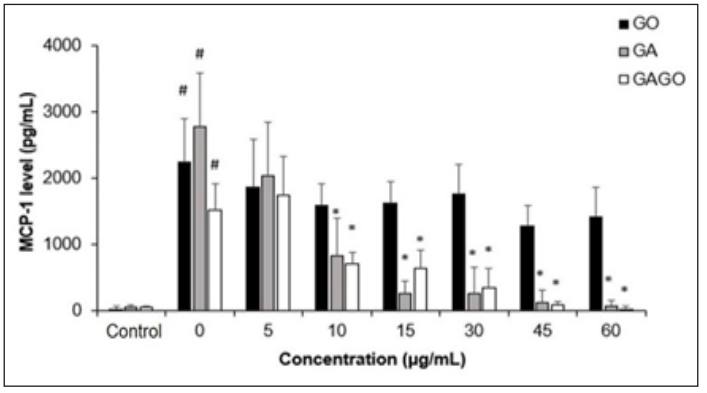

(C)

Figure 6. (A) IL-6, (B) TNF-α, and (C) MCP-1 (pg/mL) levels following treatment with GO, GA and GAGO in RAW 264.7 macrophage cells induced with LPS. RAW 264.7 cells were treated with samples at concentrations of 0-60 µg/mL for 24 h upon induction with 1 µg/mL of LPS, with non-induced cells serving as control. Significant difference of IL-6, TNF-α and MCP-1 levels to untreated cells (0 µg/mL) is denoted by (*), while (#) indicates a significant difference of control to untreated cells (0 µg/mL) ($p \leq 0.05$, $n \geq 3$)

MCP-1 levels were found to be negligible or undetectable in the uninduced cells (Control). In contrast, LPS stimulation significantly increased the levels of IL-6, TNF-α, and MCP-1 in untreated cells (0 μg/mL across all samples), indicating that LPS stimulation primarily accounted for the production of these pro-inflammatory cytokines. GA demonstrated a significant reduction of the IL-6 level in a concentration-dependent manner, as shown in Figure 6A. This reduction was significant when compared to 0 μg/mL at a concentration as low as 5 μg/mL. GAGO and GO, on the other hand, only exhibited a significantly reduced IL-6 level at 45 and 60 μg/mL. As depicted in Figure 6B, GO did not affect TNF-α levels, in contrast to the consistent decreases observed in GA- and GAGO-treated cells, with significant reductions at 10 μg/mL for GA and 15 μg/mL for GAGO. Similar to the observation of GO in TNF-α, GO did not affect the level of MCP-1, as illustrated in Figure 6C. Both GA and GAGO exhibited a significant decline in MCP-1 levels, with reductions observed starting at 10 μg/mL.

DISCUSSIONS

GAGO demonstrates reduced cytotoxicity compared to GA, indicating improved cellular compatibility up to 72 h of exposure period. One possible explanation is that interactions between GAGO and protein in the culture medium may alter the nanocomposite's surface properties and its interaction with the cells. In a previous study (Shamsi et al., 2022), the presence of protein corona on the surface of GAGO in DMEM with 10% FBS was apparent with small micellar particles (20-50 nm) observed under TEM. Protein adsorption could alter the physicochemical properties of GAGO, such as its surface charge and size, thereby modifying its "biological identity" and preventing recognition by immune cells. This influences the intracellular uptake of GAGO by macrophage cells (Cagliani et al., 2019). Protein corona formation on the surface of GAGO hinders the formation of aggregation, preventing recognition and phagocytosis by macrophage cells (Park et al., 2023).

A key finding of the present study was the ability of GA to elevate the level of NO at concentrations≥30 μg/mL, in contrast to GO and GAGO. This increase in NO could be attributed to rapid GA scavenging by cells and GA's pro-oxidant effects (Locatelli et al., 2013; Russell et al., 2012). This results in an exacerbated level of oxidative stress that activates the NF-κB signalling pathway, inducing iNOS expression and increasing NO production (Cheng et al., 2018; Wang et al., 2017), leading to cellular damage (Hassani et al., 2020). Supporting this mechanism, previous in vivo work from our laboratory demonstrated elevated ROS levels in GA-treated zebrafish embryos at higher concentrations (Ghafor et al., 2020). Li et al. (2023a) reported that GA reduced NO production through inhibition of the NF-κB signalling pathway in LPS-induced RAW 264.7 cells. At 100 μM GA (equivalent to 17.012 μg/mL), they observed NO levels of approximately 5-6 μM. This is comparable to the NO level of 5.89 μM observed in the present study at 15 μg/mL GA,

indicating agreement between the studies at similar concentrations. However, Li et al. (2023a) did not investigate the higher GA concentrations examined in the present study, where a significant increase in NO production was observed at concentrations above 30 μg/mL. Hence, it may suggest that the concentration of GA will crucially determine the extent of its anti-inflammatory effects. In contrast, GAGO has significantly suppressed NO production at 5 μg/mL, while no significant increase was observed at higher concentrations compared with the LPS-induced control (0 μg/mL). This indicates that nanocomposite formulation is able to modulate the release of GA, preventing rapid intracellular accumulation and limiting pro-oxidant activation. The controlled-release profile of GAGO may therefore prevent the sudden intracellular concentration spikes that are responsible for NF-κB overactivation (Shamsi et al., 2022).

As shown in Figure 6, GO reduced IL-6 levels but did not significantly affect TNF-α or MCP-1 levels under the conditions tested. Previous studies have shown that GO can produce different inflammatory responses depending on its physicochemical characteristics and the cell model used. For example, Feito et al. (2014) reported that six-arm PEG-functionalised GO increased TNF-α secretion in RAW 264.7 macrophages without significantly altering IL-6 or IL-1β levels. In the same study, reduced IL-6 levels were observed in stimulated primary splenocytes, highlighting that responses may differ between cell models and GO formulations. Hoyle et al. (2018) also reported reduced IL-6 without a corresponding reduction in TNF-α in a macrophage model, providing a relevant comparison with the selective IL-6 reduction observed here. In addition, Luo et al. (2020) found that GO size influenced inflammatory mediator responses in THP-1 macrophages, including effects on IL-6 and MCP-1. These findings provide broader evidence that GO can influence cytokine responses, although the differences in GO formulation and cell model mean that they do not directly explain the selective IL-6 response observed in the present study. The absence of a significant effect on MCP-1 should therefore be interpreted as an experimental finding rather than evidence of a specific pathway effect. Although TNF-α can participate in the regulation of MCP-1 production, the lack of a significant change in either mediator does not establish a shared mechanism in this study. Further studies are required to determine the mechanisms underlying the cytokine response to GO.

GA is a polyphenolic compound with reported antioxidant and anti-inflammatory activities (Badhani et al., 2015). Previous studies have shown that GA can reduce the production of inflammatory cytokines, including IL-6 and TNF-α, in experimental models of inflammation (Li et al., 2023a; Wu et al., 2022). Its anti-inflammatory activity has been proposed to involve attenuation of oxidative stress and modulation of inflammatory signalling pathways (Badhani et al., 2015). Li et al. (2023a) reported that GA at 100 μM (equivalent to 17.02 μg/mL) inhibited the secretion of IL-6 and TNF-α. In the present study, GA was evaluated over a broader concentration range of 5-60 μg/mL, and reductions in

both cytokines were observed at concentrations of 5 and 10 µg/mL and above, respectively. The reduction is also consistently exhibited at higher concentrations (Figure 6). This pattern agrees with the cytokine-reducing effects reported by Li et al. (2023a), who tested GA at 100 µM (equivalent to 17.02 µg/mL). Wu et al. (2022) also reported dose-dependent reductions in IL-6 and TNF-α in a rat model of acute inflammation, providing additional evidence that GA's effects may vary with concentration.

A critical finding of this study is the overlapping inhibition profiles of the GAGO nanocomposite, which mirror the selective behaviours of its individual components. Specifically, the IL-6 inhibition pattern under GAGO treatment closely resembles that of pristine GO, whereas the suppression patterns of TNF-α and MCP-1 align more closely with the behaviour of GA. This hybrid performance could be explained by a bifunctional, controlled-release mechanism inherent to the GAGO nanoarchitecture (Shamsi et al., 2022). At lower composite concentrations (10-30 µg/mL), the initial release of GA provides a localised concentration sufficient to canonically inhibit the upstream MAPK and NF-κB pathways. This is observed by the significant reduction in TNF-α and MCP-1 levels. Concurrently, the remaining signalling elements and post-transcriptional mRNA stabilisation machinery are robust enough to maintain IL-6 protein levels at these lower thresholds, rendering the early IL-6 response unaffected. As the concentration of GAGO increases to 45-60 µg/mL, this could cause a shift in the molecular mechanism. The internalisation of the GAGO nanocomposite (Dąbrowski et al., 2023), combined with an increased intracellular payload accumulation of released GA (Shamsi et al., 2022), triggers the activation of the Nrf2 pathway (Hoyle et al., 2018). In combination with the general shutdown of the NF-κB/MAPK engine, the synthesis of IL-6 was also completely inhibited. This dual-action, concentration-dependent kinetic framework explains why all three cytokines are suppressed at higher concentrations, establishing GAGO as a highly tunable, anti-inflammatory platform.

Despite promising findings, the present study is only limited to in vitro assessment. The molecular signalling pathways involved (e.g., NF-κB, MAPK, PI3K/Akt) were not directly investigated. Additionally, long-term stability beyond 90 days and in vivo pharmacokinetics remain to be evaluated. Future studies should focus on mechanistic pathway validation, controlled release kinetics, and in vivo efficacy models to further establish the translational potential of GAGO.

CONCLUSION

The findings from the present study collectively demonstrate improved biocompatibility of GAGO in NIH-3T3 fibroblasts and RAW 264.7 macrophages compared with native GA. GAGO also shows promising potential for anti-inflammatory effects, with significant modulation of NO levels and pro-inflammatory cytokines, namely IL-6, TNF-α, and

MCP-1. The present study provides a strong, fundamental basis for further development of GAGO in clinical settings. However, future study is warranted to assess the molecular mechanism, long-term stability and in vivo pharmacokinetics and pharmacodynamics of the GAGO nanocomposite.

ACKNOWLEDGEMENT

The authors would like to acknowledge the funding received from the Ministry of Higher Education, Malaysia, under the fundamental research grant scheme (FRGS/2018/SKK11/UPM/02/1 and FRGS/1/2023/WAB04/UPM/02/21) as well as from Universiti Putra Malaysia (GP-IPS/2023/9742000).

REFERENCES

Arip, M., Selvaraja, M., Mogana, R., Tan, L. F., Leong, M. Y., Tan, P. L., Yap, V. L., Chinnapan, S., Tat, N. C., Abdullah, M., Dharmendra, K., & Jubair, N. (2022). Review on plant-based management in combating antimicrobial resistance: Mechanistic perspective. *Frontiers in Pharmacology, 13*, Article 879495. https://doi.org/10.3389/fphar.2022.879495

Ashrafizadeh, M., Zarrabi, A., Mirzaei, S., Hashemi, F., Samarghandian, S., Zabolian, A., Hushmandi, K., Ang, H. L., Sethi, G., Kumar, A. P., Ahn, K. S., Nabavi, N., Khan, H., Makvandi, P., & Varma, R. S. (2021). Gallic acid for cancer therapy: Molecular mechanisms and boosting efficacy by nanoscopical delivery. *Food and Chemical Toxicology, 157*, Article 112576. https://doi.org/10.1016/j.fct.2021.112576

Azhari, A. (2023). *Gallic acid-loaded graphene oxide (GAGO) accelerates wound healing in in vitro and in vivo full-thickness excision wound models* [Unpublished master's thesis]. Universiti Putra Malaysia.

Bai, J., Zhang, Y., Tang, C., Hou, Y., Ai, X., Chen, X., Zhang, Y., Wang, X., & Meng, X. (2021). Gallic acid: Pharmacological activities and molecular mechanisms involved in inflammation-related diseases. *Biomedicine & Pharmacotherapy, 133*, Article 110985. https://doi.org/10.1016/j.biopha.2020.110985

Badhani, B., Sharma, N., & Kakkar, R. (2015). Gallic acid: A versatile antioxidant with promising therapeutic and industrial applications. *RSC Advances, 5*(35), 27540-27557. https://doi.org/10.1039/C5RA01911G

Cagliani, R., Gatto, F., & Bardi, G. (2019). Protein adsorption: A feasible method for nanoparticle functionalization? *Materials, 12*(12), Article 1991. https://doi.org/10.3390/ma12121991

Chen, J. S., Alfajaro, M. M., Chow, R. D., Wei, J., Filler, R. B., Eisenbarth, S. C., & Wilen, C. B. (2021). Nonsteroidal anti-inflammatory drugs dampen the cytokine and antibody response to SARS-CoV-2 infection. *Journal of Virology, 95*(7), Article e00014-21. https://doi.org/10.1128/JVI.00014-21

Cheng, Y., Li, X., Tse, H. F., & Rong, J. (2018). Gallic acid-L-leucine conjugate protects mice against LPS-induced inflammation and sepsis via correcting proinflammatory lipid mediator profiles and oxidative stress. *Oxidative Medicine and Cellular Longevity, 2018*, Article 1081287. https://doi.org/10.1155/2018/1081287

Chikere, C. O., Faisal, N. H., Kong-Thoo-Lin, P., & Fernandez, C. (2020). Interaction between amorphous zirconia nanoparticles and graphite: Electrochemical applications for gallic acid sensing using carbon paste electrodes in wine. *Nanomaterials, 10*(3), Article 537. https://doi.org/10.3390/nano10030537

Chopra, H., Dey, P. S., Das, D., Bhattacharya, T., Shah, M., Mubin, S., Maishu, S. P., Akter, R., Rahman, M. H., Karthika, C., Murad, W., Qusty, N., Qusti, S., Alshammari, E. M., Batiha, G. E.-S., Altalbawy, F. M. A., Albooq, M. I. M., & Alamri, B. M. (2021). Curcumin nanoparticles as promising therapeutic agents for drug targets. *Molecules, 26*(16), Article 4998. https://doi.org/10.3390/molecules26164998

Dąbrowski, B., Żuchowska, A., & Brzózka, Z. (2023). Graphene oxide internalization into mammalian cells: A review. *Colloids and Surfaces B: Biointerfaces, 221*, Article 112998. https://doi.org/10.1016/j.colsurfb.2022.112998

Díez-Pascual, A. M. (2021). Carbon-based nanomaterials. *International Journal of Molecular Sciences, 22*(14), Article 7726. https://doi.org/10.3390/ijms22147726

Drożdżal, S., Lechowicz, K., Szostak, B., Rosik, J., Kotfis, K., Machoy-Mokrzyńska, A., Białecka, M., Ciechanowski, K., & Gawrońska-Szklarz, B. (2021). Kidney damage from nonsteroidal anti-inflammatory drugs—Myth or truth? Review of selected literature. *Pharmacology Research & Perspectives, 9*(4), Article e00817. https://doi.org/10.1002/prp2.817

Feito, M. J., Vila, M., Matesanz, M. C., Linares, J., Gonçalves, G., Marques, P. A. A. P., Vallet-Regí, M., Rojo, J. M., & Portolés, M. T. (2014). *In vitro* evaluation of graphene oxide nanosheets on immune function. *Journal of Colloid and Interface Science, 432*, 221-228. https://doi.org/10.1016/j.jcis.2014.07.004

Grabarczyk, M., Justyńska, W., Czpakowska, J., Smolińska, E., Bielenin, A., Glabinski, A., & Szpakowski, P. (2024). Role of plant phytochemicals: Resveratrol, curcumin, luteolin and quercetin in demyelination, neurodegeneration, and epilepsy. *Antioxidants, 13*(11), Article 1364. https://doi.org/10.3390/antiox13111364

Ghafor, A. A. H. A., Elias, N., Shamsi, S., Yasin, F. M., & Sarchio, S. N. E. (2020). Toxicity assessment of gallic acid loaded graphene oxide (GAGO) nano-formulation in zebrafish (*Danio rerio*) embryos. *Pertanika Journal of Science and Technology, 28*(1), 311-326.

Gunaydin, C., & Bilge, S. S. (2018). Effects of nonsteroidal anti-inflammatory drugs at the molecular level. *Eurasian Journal of Medicine, 50*(2), 116-121. https://doi.org/10.5152/eurasianjmed.2018.0010

Hassani, A., Azarian, M. M. S., Ibrahim, W. N., & Hussain, S. A. (2020). Preparation, characterization and therapeutic properties of gum arabic-stabilized gallic acid nanoparticles. *Scientific Reports, 10*(1), Article 17808. https://doi.org/10.1038/s41598-020-71175-8

Hoyle, C., Rivers-Auty, J., Lemarchand, E., Vranic, S., Wang, E., Buggio, M., Rothwell, N. J., Allan, S. M., Kostarelos, K., & Brough, D. (2018). Small, thin graphene oxide is anti-inflammatory activating nuclear factor erythroid 2-related factor 2 via metabolic reprogramming. *ACS Nano, 12*(12), 11949-11962. https://doi.org/10.1021/acsnano.8b03642

Jiang, R., Lv, Y., Chen, B., Wu, X., Zou, Y., & Liang, L. (2024). Antioxidant effect of gallic acid on retinal ganglion cells in glaucoma model. *Scientific Reports, 14*(1), Article 14907. https://doi.org/10.1038/s41598-024-65965-7

Kumara, G. R. A., Pitawala, H. M. G. T. A., Karunarathne, B., Mantilaka, M. G. P. G. M., Rajapakse, G. R., Huang, H.-H., De Silva, K. K. H., & Yoshimura, M. (2021). Development of a chemical-free floatation technology for the purification of vein graphite and characterization of the products. *Scientific Reports, 11*(1), Article 22713. https://doi.org/10.1038/s41598-021-02101-9

Laurindo, L. F., de Carvalho, G. M., de Oliveira Zanuso, B., Figueira, M. E., Direito, R., de Alvares Goulart, R., Buglio, D. S., & Barbalho, S. M. (2023). Curcumin-based nanomedicines in the treatment of inflammatory and immunomodulated diseases: An evidence-based comprehensive review. *Pharmaceutics, 15*(1), Article 229. https://doi.org/10.3390/pharmaceutics15010229

Li, K., Gong, Q., Lu, B., Huang, K., Tong, Y., Mutsvene, T. E., Lin, M., Xu, Z., Lu, F., Li, X., & Hu, L. (2023a). Anti-inflammatory and antioxidative effects of gallic acid on experimental dry eye: *In vitro* and *in vivo* studies. *Eye and Vision, 10*(1), Article 17. https://doi.org/10.1186/s40662-023-00334-5

Li, X., Xue, X., Jia, J., Zou, X., Guan, Y., Zhu, L., & Wang, Z. (2023b). Non-steroidal anti-inflammatory drug diclofenac accelerates the emergence of antibiotic resistance via mutagenesis. *Environmental Pollution, 326*, Article 121457. https://doi.org/10.1016/j.envpol.2023.121457

Locatelli, C., Filippin-Monteiro, F. B., Centa, A., & Creczynski-Pasa, T. B. (2013). Antioxidant, antitumoral and anti-inflammatory activities of gallic acid. In M. A. Thompson & P. B. Collins (Eds.), *Handbook on gallic acid: Natural occurrences, antioxidant properties and health implications* (4th ed., pp. 1-23). Nova Science Publishers.

Lou, M., Zhang, L. N., Ji, P. G., Feng, F. Q., Liu, J. H., Yang, C., Li, B. F., & Wang, L. (2016). Quercetin nanoparticles induced autophagy and apoptosis through AKT/ERK/Caspase-3 signaling pathway in human neuroglioma cells: *In vitro* and *in vivo*. *Biomedicine & Pharmacotherapy, 84*, 1-9. https://doi.org/10.1016/j.biopha.2016.08.055

Luo, Y., Peng, J., Huang, C., & Cao, Y. (2020). Graphene oxide size-dependently altered lipid profiles in THP-1 macrophages. *Ecotoxicology and Environmental Safety, 199*, Article 110714. https://doi.org/10.1016/j.ecoenv.2020.110714

Mao, X., Wu, L. F., Zhao, H. J., Liang, W. Y., Chen, W. J., Han, S. X., Qi, Q., Cui, Y. P., Li, S., Yang, G. H., Shao, Y. Y., Zhu, D., Wang, R. F., You, Y., & Zhang, L. Z. (2016). Transport of corilagin, gallic acid, and ellagic acid from *Fructus Phyllanthi* tannin fraction in Caco-2 cell monolayers. *Evidence-Based Complementary and Alternative Medicine, 2016*, Article 9205379. https://doi.org/10.1155/2016/9205379

Marcano, D. C., Kosynkin, D. V., Berlin, J. M., Sinitskii, A., Sun, Z., Slesarev, A., Alemany, L. B., Lu, W., & Tour, J. M. (2010). Improved synthesis of graphene oxide. *ACS Nano, 4*(8), 4806-4814. https://doi.org/10.1021/nn1006368

Park, S., Ha, M. K., Lee, Y., Song, J., & Yoon, T. H. (2023). Effects of immune cell heterogeneity and protein corona on the cellular association and cytotoxicity of gold nanoparticles: A single-cell-based, high-dimensional mass cytometry study. *ACS Nanoscience Au, 3*(4), 323-334. https://doi.org/10.1021/acsnanoscienceau.3c00001

Parvin, M. S., Islam, M. S., Rahman, M. M., & Uddin, M. J. (2025). Quercetin-loaded polymeric nanoparticles inhibit PI3K/Akt signalling pathway in inflammatory cells. *International Journal of Biological Macromolecules, 260*, Article 123488.

Pasquet, P. L., Julien-David, D., Zhao, M., Villain-Gambier, M., & Trébouet, D. (2024). Stability and preservation of phenolic compounds and related antioxidant capacity from agro-food matrix: Effect of pH and atmosphere. *Food Bioscience, 57*, Article 103586. https://doi.org/10.1016/j.fbio.2024.103586

Petrovic, S., Bita, B., & Barbinta-Patrascu, M. E. (2024). Nanoformulations in pharmaceutical and biomedical applications: Green perspectives. *International Journal of Molecular Sciences, 25*(11), Article 5842. https://doi.org/10.3390/ijms25115842

Reckziegel, P., Dias, V. T., Benvegnú, D. M., Boufleur, N., Barcelos, R. C. S., Segat, H. J., Pase, C. S., dos Santos, C. M. M., Flores, E. M. M., & Bürger, M. E. (2016). Antioxidant protection of gallic acid against toxicity induced by Pb in blood, liver and kidney of rats. *Toxicology Reports, 3*, 351-356. https://doi.org/10.1016/j.toxrep.2016.02.005

Russell, L. H., Mazzio, E., Badisa, R. B., Zhu, Z. P., Agharahimi, M., Oriaku, E. T., & Goodman, C. B. (2012). Autoxidation of gallic acid induces ROS-dependent death in human prostate cancer LNCaP cells. *Anticancer Research, 32*(5), 1595-1602.

Samuelsson, I. P., & Pramling, N. (2016). Variation theory of learning and developmental pedagogy: Two context-related models of learning grounded in phenomenography. *Scandinavian Journal of Educational Research, 60*(3), 286-295. https://doi.org/10.1080/00313831.2015.1120232

Sabouripour, F., & Roslan, S. (2015). Resilience, optimism and social support among international students. *Asian Social Science, 11*(15), 159-170. https://doi.org/10.5539/ass.v11n15p159

Seisenbaeva, G. A., Ali, L. M. A., Vardanyan, A., Gary-Bobo, M., Budnyak, T. M., Kessler, V. G., & Durand, J. O. (2021). Mesoporous silica adsorbents modified with amino polycarboxylate ligands: Functional characteristics, health and environmental effects. *Journal of Hazardous Materials, 406*, Article 124698. https://doi.org/10.1016/j.jhazmat.2020.124698

Shamsi, S., Alagan, A. A., Sarchio, S. N. E., & Md Yasin, F. (2020). Synthesis, characterization, and toxicity assessment of Pluronic F127-functionalized graphene oxide on the embryonic development of zebrafish (*Danio rerio*). *International Journal of Nanomedicine, 15*, 8311-8329. https://doi.org/10.2147/IJN.S271159

Shamsi, S., Elias, N., Sarchio, S. N. E., & Md Yasin, F. (2018). Gallic acid loaded graphene oxide based nanoformulation (GAGO) as potential anti-bacterial agent against *Staphylococcus aureus*. *Materials Today: Proceedings, 5*, S160-S165. https://doi.org/10.1016/j.matpr.2018.08.059

Shamsi, S., Ghafor, A. A. H. A., Norjoshukrudin, N. H., Ng, I. M. J., Abdullah, S. N. S., Sarchio, S. N. E., Yasin, F. M., Gani, S. A., & Desa, M. N. M. (2022). Stability, toxicity, and antibacterial potential of gallic acid-loaded graphene oxide (GAGO) against methicillin-resistant *Staphylococcus aureus* (MRSA) strains. *International Journal of Nanomedicine, 17*, 5781-5807. https://doi.org/10.2147/IJN.S369373

Siu, F. Y., Ye, S., Lin, H., & Li, S. (2018). Galactosylated PLGA nanoparticles for the oral delivery of resveratrol: Enhanced bioavailability and *in vitro* anti-inflammatory activity. *International Journal of Nanomedicine, 13*, 4133-4144. https://doi.org/10.2147/IJN.S164235

Sohrabi, F., Dianat, M., Badavi, M., Radan, M., & Mard, S. A. (2021). Gallic acid suppresses inflammation and oxidative stress through modulating Nrf2-HO-1-NF-κB signaling pathways in elastase-induced emphysema in rats. *Environmental Science and Pollution Research, 28*(40), 56822-56834. https://doi.org/10.1007/s11356-021-14513-1

Sriuttha, P., Sirichanchuen, B., & Permsuwan, U. (2018). Hepatotoxicity of non-steroidal anti-inflammatory drugs: A systematic review of randomized controlled trials. *International Journal of Hepatology, 2018*, Article 5253623. https://doi.org/10.1155/2018/5253623

Srivastava, J., Chandra, H., Nautiyal, A. R., & Kalra, S. J. S. (2014). Antimicrobial resistance (AMR) and plant-derived antimicrobials (PDAms) as an alternative drug line to control infections. *3 Biotech, 4*(5), 451-460. https://doi.org/10.1007/s13205-013-0180-y

Wang, Q., de Oliveira, E. F., Alborzi, S., Bastarrachea, L. J., & Tikekar, R. V. (2017). On mechanism behind UV-A light enhanced antibacterial activity of gallic acid and propyl gallate against *Escherichia coli* O157. *Scientific Reports, 7*(1), Article 8325. https://doi.org/10.1038/s41598-017-08449-1

Wang, Z., Sun, W., Sun, X., Wang, Y., & Zhou, M. (2020). Kaempferol ameliorates cisplatin-induced nephrotoxicity by modulating oxidative stress, inflammation and apoptosis via ERK and NF-κB pathways. *AMB Express, 10*(1), Article 58. https://doi.org/10.1186/s13568-020-00993-w

Wu, Y., Li, K., Zeng, M., Qiao, B., & Zhou, B. (2022). Serum metabolomics analysis of the anti-inflammatory effects of gallic acid on rats with acute inflammation. *Frontiers in Pharmacology, 13*, Article 830439. https://doi.org/10.3389/fphar.2022.830439

Zailan, N. F. Z., Jaganathan, N., Sandramuti, T., Sarchio, S. N. E., & Hassan, M. (2020). Inhibition of GSK-3 by tideglusib suppresses activated macrophages and inflammatory responses in lipopolysaccharide-stimulated RAW 264.7 cell line. *Malaysian Journal of Medicine and Health Sciences, 16*(Suppl. 9), 2-8.

Zhang, L., McClements, D. J., Wei, Z., Wang, G., Liu, X., & Liu, F. (2020). Delivery of synergistic polyphenol combinations using biopolymer-based systems: Advances in physicochemical properties, stability and bioavailability. *Critical Reviews in Food Science and Nutrition, 60*(12), 2083-2097. https://doi.org/10.1080/10408398.2019.1630358